10-23-2020

Modifying the Surface Chemistry and Nanostructure of Carbon Nanotubes Facilitates the Detection of Aromatic Hydrocarbon Gases

John N. Hodul
Purdue University

Allison K. Murray
Marquette University, allison.murray@marquette.edu

Nikhil F. Carneiro
Purdue University

Joseph R. Meseke
Purdue University

Jacob Morris
Purdue University

See next page for additional authors

ACS Applied Nano Materials, Vol. 3, No. 10 (October 23, 2020): 10389-10398. DOI.

Modifying the Surface Chemistry and Nanostructure of Carbon Nanotubes Facilitates the Detection of Aromatic Hydrocarbon Gases

John N. Hodul
Department of Chemistry, Purdue University, West Lafayette, Indiana
Allison K. Murray
School of Mechanical Engineering, Purdue University, West Lafayette, Indiana
Ray W. Herrick Laboratories, Purdue University, West Lafayette, Indiana
Nikhil F. Carneiro
School of Mechanical Engineering, Purdue University, West Lafayette, Indiana
Ray W. Herrick Laboratories, Purdue University, West Lafayette, Indiana
Joseph R. Meseke
School of Mechanical Engineering, Purdue University, West Lafayette, Indiana

Ray W. Herrick Laboratories, Purdue University, West Lafayette, Indiana
Jacob Morris
School of Mechanical Engineering, Purdue University, West Lafayette, Indiana
Ray W. Herrick Laboratories, Purdue University, West Lafayette, Indiana
Xinping He
Charles D. Davidson School of Chemical Engineering, Purdue University, West Lafayette, Indiana
Dmitry Zemlyanov
Birck Nanotechnology Center, Purdue University, West Lafayette, Indiana
George T.-C. Chiu
School of Mechanical Engineering, Purdue University, West Lafayette, Indiana
Ray W. Herrick Laboratories, Purdue University, West Lafayette, Indiana
James E. Braun
School of Mechanical Engineering, Purdue University, West Lafayette, Indiana
Ray W. Herrick Laboratories, Purdue University, West Lafayette, Indiana
Jeffrey F. Rhoads
School of Mechanical Engineering, Purdue University, West Lafayette, Indiana
Ray W. Herrick Laboratories, Purdue University, West Lafayette, Indiana
Birck Nanotechnology Center, Purdue University, West Lafayette, Indiana
Bryan W. Boudouris
Department of Chemistry, Purdue University, West Lafayette, Indiana
Charles D. Davidson School of Chemical Engineering, Purdue University, West Lafayette, Indiana

Abstract

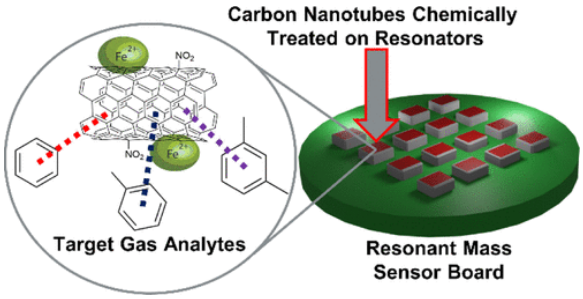

The benzene, toluene, and xylene (BTX) compounds currently utilized in many building materials and paints have been linked to deleterious health effects, and thus, monitoring the presence of these compounds is of increasing importance with respect to public health. As such, there is a critical need for next-generation low-cost, selective, and sensitive indoor BTX sensors. Current BTX detection systems require multicomponent, complex devices or require high power input to achieve BTX detection at meaningful concentrations, but this long-standing paradigm can be altered through the introduction of tailored nanomaterials. Specifically, we demonstrate a selective BTX resonant mass sensor platform that leverages the unique properties of single-walled carbon nanotubes (SWCNTs) treated with hydrochloric acid (HCl) and hydroxylamine hydrochloride (HHCl), as the resultant surface chemistry and nanostructure provides specific BTX response. That is, SWCNTs are used in this case because of their high surface area that provides a robust interaction with the target gas analyte. After the SWCNTs are treated with HCl, impurities residual from the commercial synthesis of the SWCNTs are removed, which includes reducing the amount of surface iron oxide (i.e., a residual component of the catalysis used to synthesize the SWCNTs) present into iron chlorides. There is then a following HHCl treatment that leads to the

reduction of iron(III)chloride to iron(II). This produces nitrous oxide gas, which provides a means to generate in-place surface functionalization of the SWCNTs; in turn, this allows for the selective adsorption of electron-dense aromatic analytes. Accordingly, these materials have selective interactions and unique responses toward each of the BTX analytes, and when these tailored nanomaterials are dropcast onto resonant devices, they provide for a chemically selective mass uptake response. In turn, this provides a clear pathway toward a practical, low-cost, efficient, and reusable sensor for BTX detection based on SWCNTs.

KEYWORDS:

volatile organic compounds (VOCs) sensor, functionalized carbon nanotubes, gravimetric sensor, indoor air quality monitoring

1. Introduction

Aromatic hydrocarbons, a subgroup of volatile organic compounds (VOCs), are frequently contained within consumer materials used in building interiors (e.g., paints, lacquers, adhesives, and dyes) among other settings.(1) While aromatic hydrocarbons, including benzene, toluene, and xylene (BTX), have been widely used in these various settings, these compounds have been linked to long-term deleterious health effects.(2−5) Due to their organic nature, BTX components are absorbed and are widely distributed throughout the body. For instance, acute exposure to lower concentrations of BTX compounds in air (i.e., <100 ppm) can affect the central nervous system.(6) High concentrations of BTX in air (i.e., >700 ppm) can even lead to human fatalities.(7) Additionally, BTX compounds are linked to acute myeloid leukemia and other hematological malignancies that can have long-term deleterious effects on the health and wellbeing of humans.(8,9) As a result, these chemicals are strictly regulated and monitored in many countries.(10) Given this situation, there is a pressing need for a low-cost, energy-efficient, and high-fidelity sensing platform that is tailored to have high selectivity and sensitivity for BTX compounds.

To date, various techniques have been implemented for the detection of gas-phase BTX molecules. Metal oxide-based resistive sensors, specifically, are effective in sensing BTX species.(11−14) Although effective in the detection of aromatic hydrocarbons, metal oxide resistive sensing requires high operating temperatures (i.e., >200 °C), making them impractical for many common applications.(1) As such, some groups have turned their attention to nanomaterial-based platforms. For instance, recent work focused on utilizing cobalt porphyrin-functionalized TiO_2 nanoparticles as a sensing material for BTX compounds on a suspended microheater, which allowed for lowered operating temperatures.(15) These sensors, although intriguing in the metal oxide area of BTX sensing, are limited by extensive device fabrication protocols that limit the possibility of high-throughput, low-cost fabrication processes. In addition to the metal oxide approach, there has also been work completed on BTX detection utilizing polymer and metal–organic framework materials on photonic crystal sensors, which offer low operating temperatures, but also suffer from arduous device fabrication techniques.(16,17) Conversely, the detection of aromatic hydrocarbons at low operating temperatures and using devices fabricated in methods that are consistent with solution-processing protocols has occurred with polymer-functionalized quartz crystal microbalances (QCMs).(18−21) Additionally, QCMs have shown promise with frequency counting algorithms for the selective detection of xylene at 2500 ppm.(22) However, these QCMs tend to be expensive or rely on humidity-sensitive detection methods, and these factors limit their potential to be incorporated into existing buildings and interior spaces. Moreover, photoionization detectors, amperometric detectors, semiconductors (i.e., chemiresistive sensors), flame ionization detectors, and portable gas chromatographs/mass spectrometers (GC/MS) have been implemented for the detection of aromatic hydrocarbons.(23−29) These sensors, although sensitive to BTX, lack selectivity and durability, and have high power consumption and cost.(30) Therefore, there exists a critical need for a sensor platform that can provide high chemical sensitivity and selectivity among BTX analytes without compromising reusability, cost, and power metrics.

To satisfy these demands, sensor platforms utilizing single-walled carbon nanotubes (SWCNTs) are used extensively in gas sensing applications because of their ability to provide a robust interaction with the target gas analyte and high chemical stability.(31) This strong interaction is attributed to the high surface area of the SWCNTs (>1500 $m^2 g^{-1}$) and high surface area-to-volume ratio.(32) However, when incorporating these SWCNTs into a sensing platform to target specific analytes, such as BTX, these sensors must meet certain criteria. A practical and efficient BTX gas sensor should offer: (i) high sensitivity and selectivity; (ii) a fast response time to BTX exposure and recovery time when BTX is removed (i.e., ∼1 s); (iii) a low operating temperature (i.e., near-room temperature) and temperature-independent operation; and (iv) chemical and device stability upon cycling.(33,34) To meet these sensor metrics, these nanomaterials are typically chemically-modified with various functional groups, polymers, and metal oxide nanoparticles to improve their selectivity and sensitivity to target analyte gases.(35−38) These chemical modifications allow certain SWCNT-based devices to meet the sensor criteria and provide the ability to sense target analytes selectively; however, these modifications can be costly because of the expensive functional chemistries utilized. Thus, creating a sensor platform that leverages the nanoscale advantages of SWCNTs and that satisfies the necessary sensing criteria with little to no additional cost of added materials has great value in the sensing field.

Here, a resonant mass sensor is coated with SWCNTs and then chemically treated with an inexpensive and commonly-used hydroxylamine hydrochloride (HHCl) reagent to dope the SWCNTs in a single step (Scheme 1). This doping allows for the selective detection of BTX compounds. This never-before-reported chemical functionalization protocol, in combination with the resonant mass sensor platform, allows for low-cost and practical BTX detection. In comparison to other SWCNT sensing counterparts, this sensor offers high sensitivity, low operating temperature, small size, and long-term cyclability. Using Pierce oscillators implemented with a frequency counting algorithm, the simultaneous monitoring of 16 sensors, each with a temporal resolution of 1 s and frequency resolution of ∼1 Hz, is achieved. This Pierce oscillator system with this functional chemistry allows for selective detection of BTX compounds. These functional materials require low-energy input, and they do not require humidity to perform unlike other functional materials on QCMs. Moreover, this resonant mass sensor platform offers lower cost materials to manufacture and is smaller in size, requires less cumbersome electronics and controls to perform tests, and is more portable than a standard QCM. Additionally, the chemistry and nanoscale structure of the SWCNTs allows for the detection of aromatic hydrocarbon analytes selectively because of an electron-withdrawing character that is associated with the SWCNTs after their treatment with HHCl. Thus, the apparent selective adsorption of BTX analytes is related to the electron density in each of the aromatic structures of each target analyte. The surface treatment creates minor surface alterations in the SWCNTs without any additional device manipulations to achieve BTX detection. Thus, this nanomaterials platform offers an easily functionalized, low-cost, low-power, multichannel sensing array capable of quick and reliable detection. The resonant mass sensor platform with this functional chemistry offers advantages by creating a low-cost and selective alternative to BTX detection without the need for a high-power input, extensive chemical treatment, or device manipulation protocols. Therefore, this work provides a feasible and reliable surface treatment method that, when paired with pre-existing sensor platforms, can offer robust BTX selective detection. The ease of surface treatment allows for high responses to aromatic analytes and provides a novel chemical functionalization protocol for an important class of functional nanomaterials.

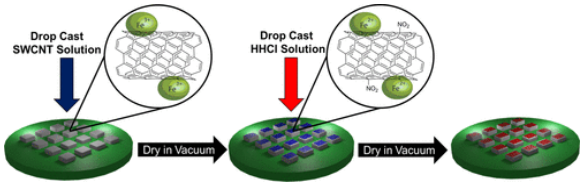

Scheme 1. Schematic of the Device Chemical Functionalization Protocol

2. Experimental Methods

2.1. Materials

All chemicals were purchased from Sigma-Aldrich, and they were used as received unless otherwise noted. High-pressure carbon monoxide (HiPco) synthesized SWCNTs were purchased from ChemElectronics Inc., and they were treated by exposing them to air at 300 °C. Then, the SWCNTs were washed with concentrated (i.e., 38%, by weight) hydrochloric acid (HCl) in water to remove some of the remaining metal catalysts prior to use.(39,40) After acid treatment, the SWCNTs were then isolated via centrifugation. SWCNT inks were prepared by dispersing the SWCNTs in a tetrahydrofuran (THF) solution at a loading of 0.1 mg mL^{-1} using a probe tip sonicator (QSonica, LLC) producing a murky dark yellow solution. Hydroxylamine hydrochloride (HHCl) was stored under nitrogen conditions in a glove box upon receipt and all of the solutions containing HHCl were prepared in the glove box.

2.2. General Methods

Raman spectra were obtained using a Horiba/Jobin-Yvon LabRAMHR800 confocal microscope Raman spectrometer equipped with a 633 nm He:Ne laser. For these spectra, the SWCNT samples were fabricated by depositing 0.5 mL of a 0.1 mg mL^{-1} SWCNT suspension onto a glass microscope slide and drying the slide under vacuum ($P \leq 0.4$ Torr) for 30 min to remove solvent. Then, the spectra were acquired before and after treatment with HHCl. For samples analyzed after the HHCl treatment, after the vacuum drying step, the SWCNT-coated substrates underwent a 1 µL treatment of either 1 or 100 mg mL^{-1} HHCl solution. These samples were then dried under vacuum again prior to testing. Optical microscopy images were acquired using a 2× telecentric lens with a color USB camera (Edmund Optics, EO-1312). The same sample preparation protocol that was utilized in obtaining the Raman spectra was utilized for this imaging as well. A Hitachi S-4800 field emission scanning electron microscope (SEM) was utilized to image the SWCNTs. For these images, 0.5 mL of the 0.1 mg mL^{-1} SWCNT solution were printed on silicon dioxide substrates and dried under vacuum for 24 h. For samples that were treated with HHCl, the HHCl was pipetted on top of the dried SWCNTs, and then these films were dried under vacuum for another 24 h. All of the films were then coated with 20 nm of carbon prior to imaging using a SPI carbon sputter coater. A Kratos Axis Ultra DLD imaging X-ray photoelectron spectrometer with a monochromatic Al Kα (E = 1486.6 eV) was utilized for X-ray photoelectron spectroscopy (XPS) measurements, and these data were acquired while the sample was under high vacuum ($P \sim 10^{-9}$ Torr). CasaXPS software was utilized for all of the XPS data analyses.

2.3. Device Instrumentation

The sensor array in this work consisted of 16 Pierce oscillators (Figure 1a). Each oscillator consisted of an inverter, two load capacitors (C_1 = 22 pF and C_2 = 22 pF), one feedback resistor (R_1 = 2 MΩ), one isolation resistor (R_2 = 510 Ω), and a quartz crystal resonator (Kyocera Corp., CX3225) with the cap removed, where the capacitance of the resonator was C_L = 12 pF. The crystal oscillator driver (Texas Instruments, SN74LVC1GX04) provided the circuit with the Pierce oscillator inverter, as well as three additional inverters, which converted the oscillator output signal to a square wave. A field programmable gate array (FPGA) was implemented as a frequency counter to track the oscillation frequency of each oscillator in parallel. This resulted in 16 parallel frequency measurements every second with a frequency resolution of 1 Hz. To improve experimental efficiency, the 16 resonators were isolated on a disposable resonator board. This was mechanically-coupled to an instrumentation board that contained the remaining elements of the oscillator circuitry. Additionally, a labeled picture of the testing instrumentation is shown in Figure S5.

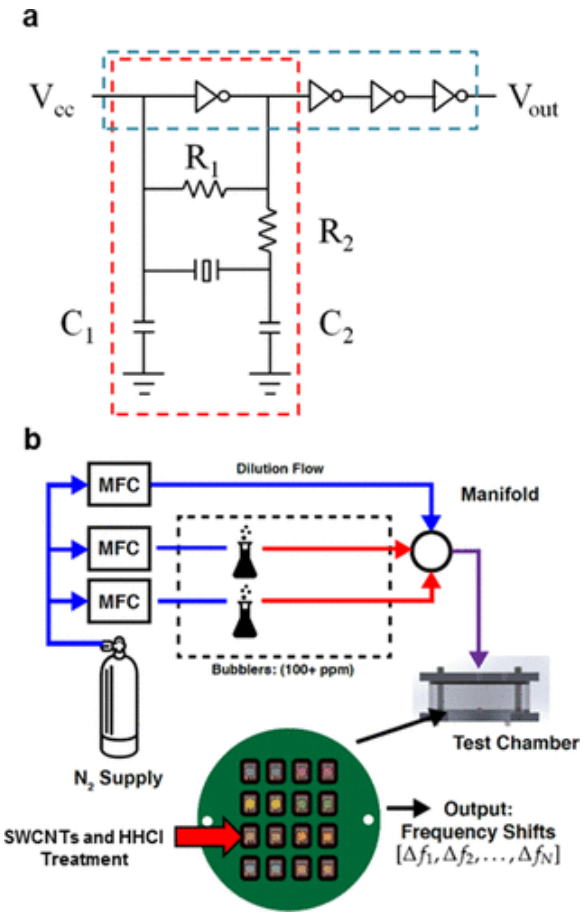

Figure 1. (a) Schematic representation of the Pierce oscillator circuit with the oscillator (outlined by red dashed lines) and a series of inverters (outlined by blue dashed lines). C_1 and C_2 are load capacitors. R_1 is a feedback resistor, and R_2 is an isolation resistor. V_{cc} is the supply voltage, and V_{out} is the output voltage that enters the FPGA frequency counter. (b) Experimental setup utilized to test the sensors exposed to the target gases. The functionalized oscillators were evaluated in a chamber filled with analyte gas from bubblers connected to mass flow controllers (MFCs) and diluted with a stream of nitrogen.

2.4. Device Functionalization

SWCNTs were functionalized with HHCl using an inkjet printer in a manner that has been reported previously.(41) In these experiments, 1 µL of the 0.1 mg mL^{-1} SWCNT in THF ink was drop cast on to the quartz crystal resonator surface. The devices were left to dry under vacuum ($P \leq 0.4$ Torr) for at least 30 min. Subsequently, 5 nL of a solution of HHCl in methanol (1 mg mL^{-1}) were printed on the resonator surface using a BioFluidix PipeJet P9 piezoelectrically-actuated pipette. After functionalization, the resonator board was stored under vacuum for at least 24 h to remove any residual solvent.

2.5. Device Testing

Testing of the devices was performed using the experimental setup shown in Figure 1b. Prior to sensor testing, the resonator board was attached to the instrumentation board, and the 9.5 cm diameter chamber was sealed. The chamber was secured with an in-line flow distribution system to achieve the desired concentrations of the analytes. Nitrogen was connected to a series of MFCs in parallel. Some of the MFCs (MKS 1480A, 40 cm^3 min^{-1}) were connected to bubblers (ChemGlass, AF-0085) with 10 mL of the desired testing analyte. An additional line (MKS 1179A, 500 cm^3 min^{-1}) remained as a pure nitrogen source. The three inlets were connected to a manifold, the output of which was connected directly to the chamber inlet. The chamber was flushed with nitrogen at a

flow rate of 500 cm^3 min^{-1} to create an inert environment as the baseline for experimentation. Subsequently, the analyte gases were injected into the chamber to achieve the reported concentrations. Simultaneously, the oscillation frequencies were recorded once per second with a 1 Hz resolution using the myRio FPGA and an in-house LabVIEW program. For all of the tests, at the beginning of the test, a longer break-in period was used such that the resonators could acclimate to the humidity and temperature of the testing chamber. This period consisted of a 60 min pulse of nitrogen at a pressure of 1 atm and a temperature of 25 °C.

3. Results and Discussion

SWCNT-based sensor platforms typically require chemical modifications or specific deposition methods to adequately meet sensing metrics. This chemical treatment can be expensive and require multiple chemical steps to provide selectivity and sensitivity among BTX analytes.(42−44) However, when a thin film of SWCNTs was treated with HHCl there was an observed selective response to the BTX analytes. Figure 2a shows the oscillation frequency responses of the SWCNT-coated resonant mass sensors after being treated with 1 mg mL^{-1} HHCl solutions. This surface chemistry allowed for the detection of BTX compounds with unique concentration-shift relationships. The average sensitivity of the device to BTX was 136, 35, and 23 ppm Hz^{-1}, respectively.

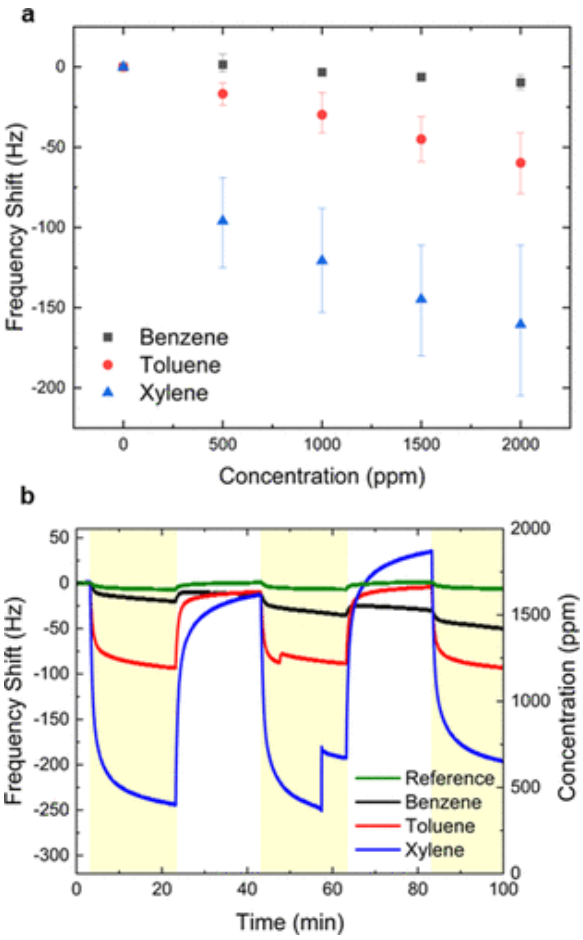

Figure 2. (a) Average shift in oscillation frequency of devices functionalized with SWCNTs and 1 mg mL^{-1} of HHCl exposed to either benzene, toluene, or xylene, as a function of increasing concentration (500 ppm ≤ *C* ≤ 2000 ppm). The error bars represent the maximum and minimum observed shifts across 4 trials. (b) Change in oscillation frequency of a device functionalized with SWCNTs and 1 mg mL^{-1} of HHCl exposed to 2000 ppm of BTX analytes as a function of time. The response of an unfunctionalized device (reference) exposed to 2000 ppm of benzene is shown in green for comparison. The yellow bars indicate the concentration of the analyte present and the white bars indicate a nitrogen-only environment.

The sensor showed specific oscillation frequency responses to BTX analytes, and this response only occurred when the treated SWCNTs were present on the resonator (i.e., the reference channel resonators did not show a meaningful response to BTX). The response time and recovery time of the sensor was determined by calculating a time constant (τ), the time it takes the sensor to reach approximately 63.2% of its final value (i.e., either on the fall for the response time or the rise for the recovery time). Here, the average response time of the sensor can be characterized by a time constant of 31 ± 15.3 s with an average recovery time constant of 49 ± 17.2 s. In this work, selectivity was defined as a characteristic response in the magnitude of oscillation frequency shift for individual analytes at a single concentration. Therefore, it is noted that this sensor cannot be used to distinguish between BTX analytes when both are present under testing conditions at the same time (e.g., xylene and benzene both being present in the testing chamber at same time). Moreover, the responses on all of the SWCNT-coated oscillators were rapid and reversible, which indicated target analytes were physically adsorbing to the devices. Importantly, the SWCNT-based sensors showed stability over multiple cycles, as the baseline signal of the resonators quickly recovered after desorption of the target analyte (Figure 2b). However, there was an observed jump in oscillation frequency when returning to the baseline value (Figure 2b). These jumps in oscillation frequency are due to an unknown frequency counter glitch. Occasionally, a jump in frequency of a single channel is seen. This is believed to be a control electronics concern exclusively and not an artifact of the functional material or sensor. Additionally, the long term stability of the functionalized resonator was determined by testing with five 30 min pulse cycles of xylene at a concentration of 2000 ppm (Figure S4). The measured frequency shift from resonators functionalized with SWCNTs and HHCl varied only approximately 10% from the initial pulse. These initial results, although intriguing, did not provide a fundamental understanding of how the sensor was responding to these target analytes.

Exposing the SWCNT thin films to the HHCl solution resulted in a decrease in the concentration of iron impurities present in the carbon nanotubes. Iron is a metal catalyst utilized in the HiPco SWCNT synthesis and, even after purification, can remain in the carbon nanotubes.(45) When chemical modifications occurred on the carbon nanotube surfaces there was typically an observed characteristic change in the Raman spectra,(46) and this was observed in the present work as well (Figure 3). In particular, the effect of a chemical interaction with the SWCNTs alters the doping levels of SWCNTs, and in turn, alters the carbon nanotube sensing ability.(44) These doping effects can be predicted based on the shifts in the G-band (λ = 1591.4 cm^{-1}) in the Raman spectrum. The G-band characteristically describes the sp^2 carbon bond character in these graphitic materials.(47) In the samples that underwent the HHCl treatment, no shifts in this G-band were observed. This indicated that no significant doping effects occurred on the surface of the SWCNTs. However, the D-band (λ = 1308.5 cm^{-1}) showed an appreciable decrease as the amount of HHCl added to the films increased. This D-band is associated with the stretching of the sp^3 carbon bond character.(48) This appreciable decrease in the D-band indicated that there was a decrease in the sp^3 C–C bond character. This is likely due to a decrease in iron impurities in the SWCNTs upon exposure to HHCl as these types of impurities can alter the amount of sp^3 C–C bond character in a carbon nanotube by distorting the sp^2 C–C bond character.(46) Additionally, this could also be due to layering effects that can produce edge defects in the carbon network.(49,50) When the iron chlorides are formed, they can become layered within the carbon nanotubes. Upon reduction of the iron chlorides with HHCl, there is an observed decrease in the D-band because the layering defects are disrupted. Hence, there is a decrease in the D band region because more sp^2 planar type character is expressed after the defects are removed.

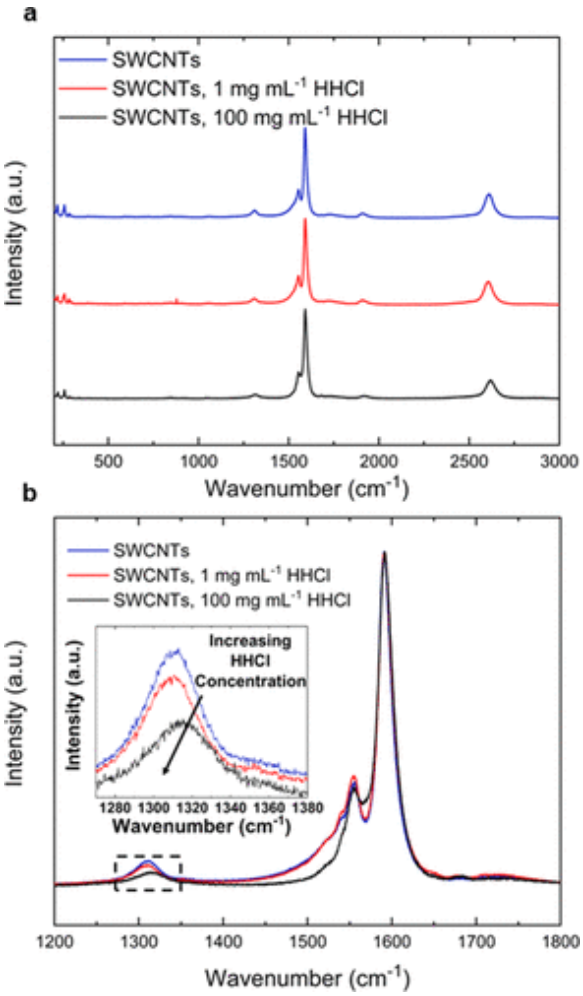

Figure 3. (a) Raman spectra comparison of SWCNTs alone (blue), after 1 mg mL^{-1} HHCl treatment (red), and after 100 mg mL^{-1} HHCl treatment (black). (b) Zoomed overlap view of Raman spectra of the G-band (λ = 1591.4 cm^{-1}) and D-band (λ = 1308.5 cm^{-1}) after the different treatments had been performed.

Moreover, when treating the SWCNTs with HHCl, there was an increase in the nitrogen signature associated with the SWCNTs according to the collected XPS data (Figure 4). From the C 1s XPS spectrum, five peaks centered at 284.5, 285.3, 285.7, 286.5, and 288.9 eV are observed, corresponding to C–C sp^2, C–C sp^3, C–N, C–O, and $FeCO_3$ groups, respectively.(51−53) After treatment with the HHCl, the intensities of C–O peaks decrease slightly, which was accompanied by an increase of the nitrogen carbon peak (C–N), revealing that the oxygen-containing groups were slightly removed or replaced with corresponding nitrogen-containing groups. This increasing C–N character is consistent with previous work describing the reduction of graphene oxide materials using HHCl.(53)

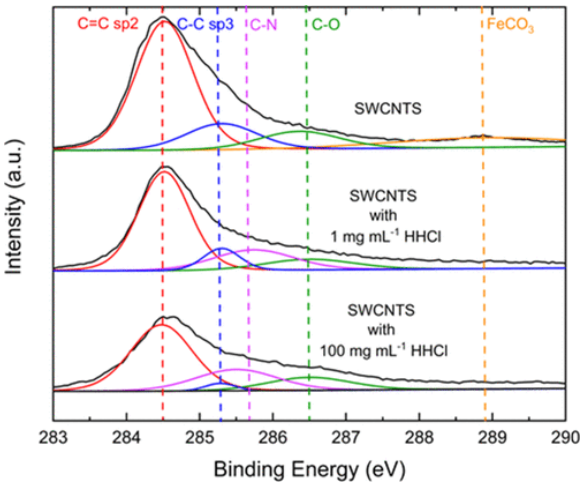

Figure 4. XPS spectra of the C 1s level of SWCNTs with increasing concentration of HHCl treatments.

There was a decrease in the C–C sp^2 and sp^3 carbon networks, which could be attributed to the incorporation of a higher concentration of noncarbonaceous materials being present around the carbon nanotubes (i.e., residual HHCl). Additionally, there was a clear loss of a $FeCO_3$ peak at 288.9 eV. This peak reduction most likely correlates to iron carbonates, which are reduced upon exposure to HHCl.(54) Such a trend is consistent with the Raman spectroscopy (*vide supra*) where there was a substantial change in the D band (1308.5 cm^{-1}), as shown in Figure 3b. However, this does indicate the presence of iron in the sample even after purification. In addition to these spectroscopic results, SEM micrograph images show an ordering of the HHCl salts when the SWCNTs are present. That is, SWCNTs cast without the HHCl treatment do not contain any regular nanostructure (Figure S1). Clear nano- and microstructures only appear when the SWCNTs are treated with the HHCl (Figures S2 and S3). Overall, the observation of increasing C–N bond character in the XPS and decreasing of iron impurities upon HHCl treatment indicates that the iron present had an impact on the sensitivity and selectivity of the device.

The high sensitivity and selectivity among BTX analytes observed in the high-performance sensors described above is likely based on the ability of the HHCl to reduce the iron impurities in the SWCNTs; in turn, this allows for the in-place synthesis of NO_2 functional groups on the surfaces of the carbon nanotubes. This reduction causes an increased formation of C–N type bond character, as observed in the XPS spectra. Residual iron metal in the HiPco SWCNTs, when heated in ambient conditions, can oxidize, and this creates a mixture of iron oxides, consisting of iron(II) and iron(III) oxides. These iron oxides, when exposed to the HCl in the purification process, can be converted into iron chlorides. Then, the SWCNTs containing iron(III) chlorides undergo a redox reaction when they are exposed to the HHCl treatment.(55) This redox reaction produces an NO_2 gas byproduct that can bind to the surface of the SWCNTs and create an electron-poor character in the graphene sheets (Scheme 2).(56−59) The change in electron density in the SWCNTs provides the selectivity among BTX analytes. As the electron density in the target analytes increases, there is better sp^2 π-stacking due to the π accepting character in the SWCNTs and the π donor character in the aromatic analytes. Therefore, the treatment of SWCNTs with HHCl provides a reliable and cost-effective selective sensor surface treatment chemistry.

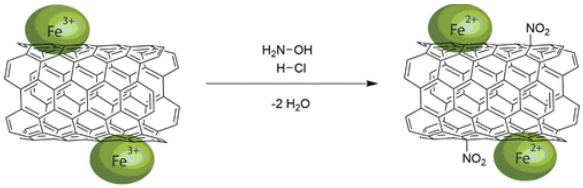

Scheme 2. Proposed Mechanism for the Production of NO_2 Functional Groups upon Treatment with HHCl

To evaluate this mechanism further, 16 devices were functionalized using combinations of two types of 0.1 mg mL^{-1} SWCNTs in THF (pure and impure) and two types of 1.0 mg mL^{-1} HHCl conditions (with and without treatment). Pure SWCNTs were treated with HCl prior to testing. "HHCl with" or "without" indicates whether the SWCNTs were treated with HHCl prior to testing. A representative response of these four functionalized types of devices and an unfunctionalized device under exposure to 2000 ppm of xylene is shown in Figure 5. The oscillators functionalized with pure SWCNTs and with HHCl treatment exhibited the largest shift in oscillation frequency to 2000 ppm xylene of 61.6 Hz. Additionally, these devices had the most consistent device-to-device performance. Therefore, SWCNTs containing iron must have iron(III) chlorides present to produce an adequate response. As shown in Figure 5, without the HCl treatment (impure) there is no formation of iron chlorides, and the device had little to no response to xylene (red and black signals in Figure 5). With the HCl treatment (pure) there was an increase in sp^2 character in the SWCNTs graphene sheets resulting in a more uniform sp^2 hybridized surface and some noncovalent response to xylene. However, it was not until HHCl treatment following the HCl treatment that there was a production of the NO_2 gas to chemically alter the SWCNTs and provide the enhanced response to xylene (magenta line in Figure 5).

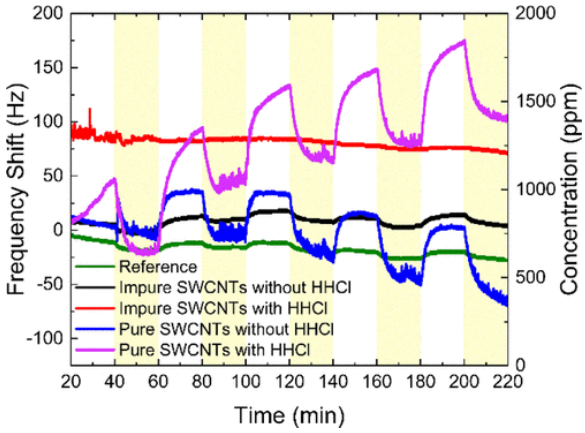

Figure 5. The oscillation frequency of an oscillator functionalized with different combinations of 0.1 mg mL^{-1} SWCNTs and 0.2 mg mL^{-1} HHCl exposed to 2000 ppm xylene. Impure SWCNTs were not treated with any HCl prior to testing. These combinations consisted of no chemistry added on the device (reference), impure SWCNTs without the HHCl treatment, impure SWCNTs with the HHCl treatment, pure SWCNTs without the HHCl treatment, and pure SWCNTs with the HHCl treatment. The yellow bars indicate the corresponding concentration of xylene in the testing chamber and the white bars indicate a nitrogen-only environment.

To determine if this electron-poor character existed in our SWCNTs, we evaluated other target aromatic analytes (Figure 6). This consisted of electron-rich aromatic compounds (i.e., trimethylbenzene, anisole, and aniline) being evaluated while xylene was used as a reference case analyte. During testing, the electron-rich analytes encountered the electron-poor SWCNTs, and the resonators showed an enhanced uptake of the electron-rich analytes relate to the xylene reference. That is, aromatic compounds with high electron densities showed a unique frequency response as they interacted with the chemically treated SWCNTs. Anisole, xylene, aniline, and trimethylbenzene showed average frequency shifts of 11.7, 14.7, 57.7, and 177.7 Hz, respectively, when fed at a concentration of 750 ppm. This supports the idea that the electron-withdrawing character created in the SWCNTs upon treatment with HHCl is indeed the reason for selectivity among aromatic analytes. The proper calibration of the device to each specific analyte allows for the chemically-selective detection of each compound, which demonstrates the versatility and applicability of this sensing platform.

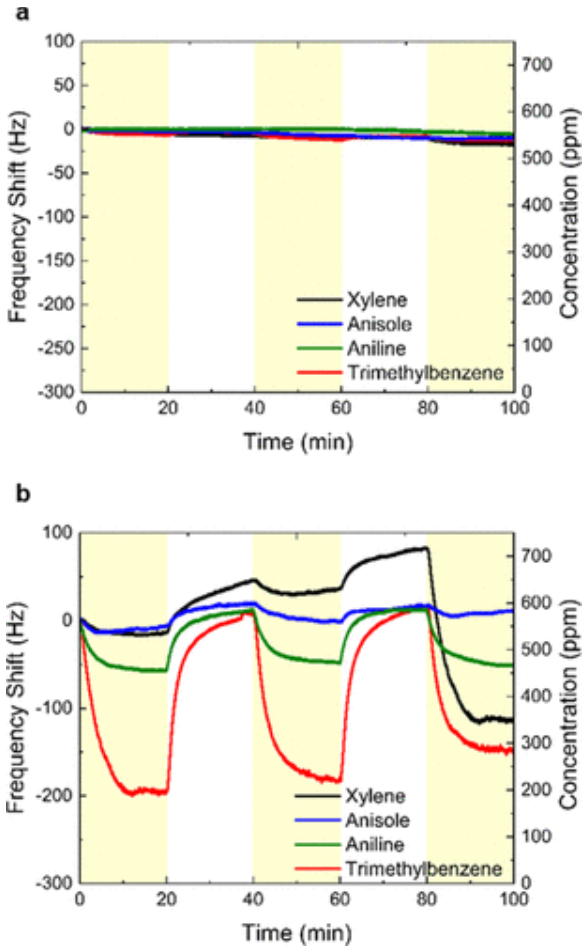

Figure 6. Shift in oscillation frequency of (a) unfunctionalized oscillator and (b) an oscillator functionalized with 1 mg mL^{-1} HHCl and SWCNTs as referenced from the initial oscillation frequency of devices exposed to 750 ppm of xylene, anisole, aniline, and trimethylbenzene with respect to time. The yellow bars indicate the concentration of the analyte with a background of nitrogen.

The functionalized resonators showed responses to aromatic hydrocarbons in relative humidity (RH) environments ranging from 0 to 80% while air was used as the carrier gas. Under these conditions, the SWCNT-based sensors showed meaningful responses to 2000 ppm of xylene with average frequency shifts of 22.1 ± 1 Hz for the 0% ≤ RH ≤ 60% RH levels (Figure 7). The responses remained reliable until the 80% RH level where the average frequency shift dropped to 16.8 Hz. Once reaching the 80% RH level, there was an observed downward drift, which we speculate was due to the accumulation of moisture on the surface of the resonator. This moisture accumulation caused a change in the oscillation frequency as a function of time. However, these results do show the applicability and practical performance of the surface functionalization chemistry in combination with this resonant mass sensor platform under conditions that could potentially exist in many indoor air quality monitoring scenarios.

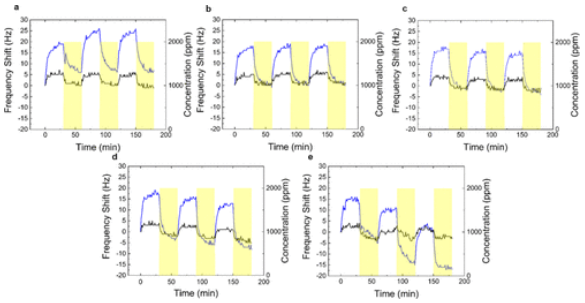

Figure 7. Change in oscillation frequency of a device functionalized with SWCNTs and 1 mg mL^{-1} of HHCl exposed to 2000 ppm of xylene as a function of time in the presence of increasing RH levels indicated by the blue line. (a) 0 (b) 20 (c) 40 (d) 60 (e) 80% RH. The response of an unfunctionalized device (reference) under same conditions at same time indicated by the black line. The yellow bars indicate the concentration of the xylene analyte present and the white bars indicate an air-only environment.

In addition to accounting for RH, practical interior environments could contain interfering volatile organic analytes that could disrupt the response to aromatic analytes. For this reason, pulses of xylene at 2000 ppm were added to the sensor while pulses of 500 ppm and 1000 ppm of either ethanol or propane were injected (Figure 8). This allowed us to establish how the response to xylene was impacted in the presence of interfering VOC agents. Figure 8a shows the response of functionalized and unfunctionalized (i.e., uncoated resonator) devices without any xylene present for comparison. Figure 8b shows the response of a functionalized device with xylene present.

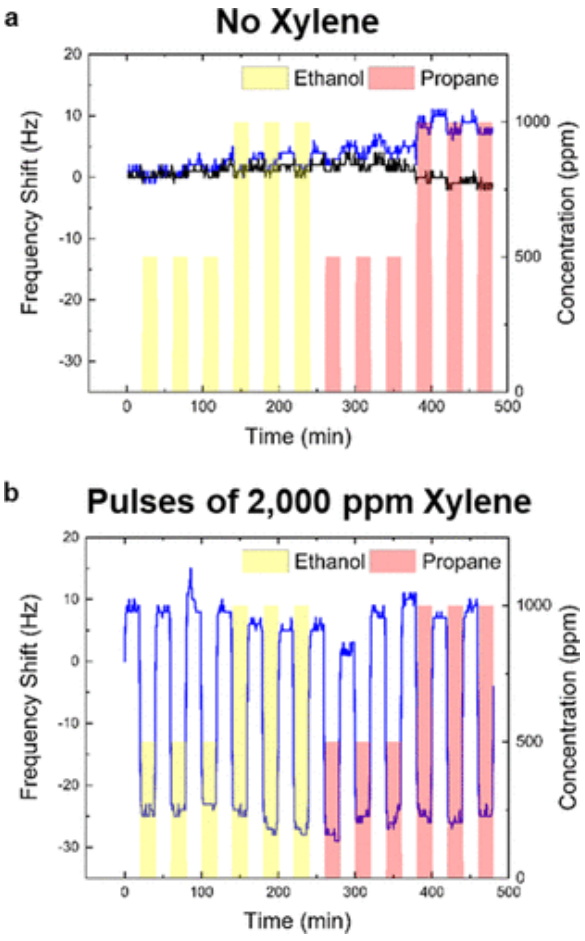

Figure 8. The change in oscillation frequency of a device functionalized with SWCNTs and 1 mg mL^{-1} of HHCl exposed to (a) ethanol and propane pulses as a function of time indicated by the blue line. The response of an

unfunctionalized device (reference) under same conditions at the same time is indicated by the black line. (b) Ethanol and propane with 2000 ppm of xylene pulses as a function of time indicated by the blue line.

This sensor only showed responses when xylene was present and showed similar responses in the presence of the interfering gases relative to when the distractant gases were not present (Figure 8b). That is, this materials combination shows a selective responsive towards the detection of aromatic gases over other potential gas analyte chemistries. These results demonstrate that this sensor can be utilized in interior locations where interfering gases could potentially be present without disrupting BTX detection.

To determine the limit of detection capability of this platform to a specific aromatic compound, xylene, the device response at 100 ppm of xylene in nitrogen was monitored (Figure 9). The SWCNT-based device was able to show a frequency shift response to xylene at 100 ppm that is greater than the response of the reference channel with a sensitivity of 4 ppm Hz^{-1}. Additionally, this device remained reusable even at this concentration because of the adsorption and desorption pathways occurring when nitrogen gas is purged into the testing chamber. This device offers a feasible and practical surface chemistry that can selectively respond to aromatic compounds at quantitative levels.

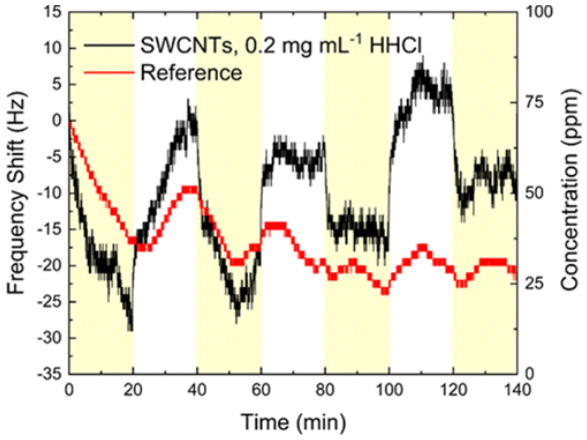

Figure 9. The oscillation frequency of an oscillator functionalized with 0.2 mg mL^{-1} of HHCl and 0.1 mg mL^{-1} SWCNTs exposed to 100 ppm of xylene in nitrogen. The black lines and red lines represent the oscillation frequency of the functionalized and unfunctionalized device (reference) in response to xylene, respectively. The yellow bars indicate the concentration of the analyte present and the white bars indicate a nitrogen-only environment.

4. Conclusions

This work leveraged SWCNTs treated with HHCl for enhanced selective BTX sensing when they were incorporated into a resonant device. The HCl treatment followed by an HHCl treatment on the SWCNTs allowed for an enhanced interaction with aromatic analytes, and thus, yielded a greater response. This carbon nanotube treatment chemistry reduces iron(III) chloride and allows for the electron withdrawing-type character in the SWCNTs due to the NO_2 gas released. This surface chemistry and resonant mass sensor combination provides a robust sensor and practical monitoring of BTX compounds, as well as other aromatic compounds. Furthermore, the oscillator-based approach allowed for the detection of xylene at 100 ppm. Additionally, low-cost components and functional materials integrated with additive manufacturing resulted in an efficient, reusable, economical, and feasible BTX sensing platform. This work combined a feasible chemical treatment protocol with the practical implementation of the resonant mass sensors to create a robust sensing platform suitable for the detection of aromatic analytes. Therefore, this effort allows for a processable chemistry to be applied in a new manner to detect aromatic hydrocarbons using advanced nanomaterials. This nanomaterials system, when

combined with a straightforward treatment protocol, offers a unique option in the sensors community to improve BTX gas detection using low-cost, high-throughput processing techniques of carbon nanotubes. Importantly, these nanomaterials easily could be incorporated into existing sensor manufacturing efforts to provide efficient and effective indoor air monitoring devices on a relatively rapid timescale.

Supporting Information

The Supporting Information is available free of charge at https://pubs.acs.org/doi/10.1021/acsanm.0c02295.

- SEM images of the treated and untreated SWCNT thin films; a plot demonstrating the stability of the devices under operation; and photographs showing the experimental setup used to evaluate the nanomaterial-based sensing devices (PDF)

Terms & Conditions

Notes

The authors declare no competing financial interest.

Acknowledgments

This work was funded by the Center for High Performance Buildings at Purdue University (grant number: CHPB-44-2019).

References

1 Mirzaei, A.; Kim, J.-H.; Kim, H. W.; Kim, S. S. Resistive-Based Gas Sensors for Detection of Benzene, Toluene and Xylene (BTX) Gases: A Review. *J. Mater. Chem. C* **2018**, *6*, 4342– 4370, DOI: 10.1039/c8tc00245b

2 Ware, J. H.; Spengler, J. D.; Neas, L. M.; Samet, J. M.; Wagner, G. R.; Coultas, D.; Ozkaynak, H.; Schwab, M. Respiratory and Irritant Health Effects of Ambient Volatile Organic Compounds: The Kanawha County Health Study. *Am. J. Epidemiol.* **1993**, *137*, 1287– 1301, DOI: 10.1093/oxfordjournals.aje.a116639

3 Molhave, L. Volatile Organic Compounds, Indoor Air Quality and Health. *Indoor Air* **1991**, *1*, 357– 376, DOI: 10.1111/j.1600-0668.1991.00001.x

4 de Gennaro, G.; Farella, G.; Marzocca, A.; Mazzone, A.; Tutino, M. Indoor and Outdoor Monitoring of Volatile Organic Compounds in School Buildings: Indicators Based on Health Risk Assessment to Single out Critical Issues. *Int. J. Environ. Res. Public Health* **2013**, *10*, 6273– 6291, DOI: 10.3390/ijerph10126273

5 Holcomb, L. C.; Seabrook, B. S. Review: Indoor Concentrations of Volatile Organic Compounds: Implications for Comfort, Health and Regulation. *Indoor Environ.* **1995**, *4*, 7– 26, DOI: 10.1177/1420326x9500400103

6 Chen, M.; Wang, Z.; Han, D.; Gu, F.; Guo, G. Porous ZnO Polygonal Nanoflakes: Synthesis, Use in High-Sensitivity NO_2 Gas Sensor, and Proposed Mechanism of Gas Sensing. *J. Phys. Chem. C* **2011**, *115*, 12763– 12773, DOI: 10.1021/jp201816d

7 Gist, G. L.; Burg, J. R. Benzene—A Review of the Literature from a Health Effects Perspective. *Toxicol. Ind. Health* **1997**, *13*, 661– 714, DOI: 10.1177/074823379701300601

8 Lan, Q.; Zhang, L.; Li, G.; Vermeulen, R.; Weinberg, R. S.; Dosemeci, M.; Rappaport, S. M.; Shen, M.; Alter, B. P.; Wu, Y.Hematotoxicity in Workers Exposed to Low Levels of Benzene. *Science* **2004**, *306*, 1774– 1776, DOI: 10.1126/science.1102443

9 McHale, C. M.; Zhang, L.; Smith, M. T. Current Understanding of the Mechanism of Benzene-Induced Leukemia in Humans: Implications for Risk Assessment. *Carcinogenesis* **2012**, *33*, 240– 252, DOI: 10.1093/carcin/bgr297

10 Lin, T.; Lv, X.; Hu, Z.; Xu, A.; Feng, C. Semiconductor Metal Oxides as Chemoresistive Sensors for Detecting Volatile Organic Compounds. *Sensors* **2019**, *19*, 233, DOI: 10.3390/s19020233

11 Qu, F.; Shang, W.; Wang, D.; Du, S.; Thomas, T.; Ruan, S.; Yang, M. Coordination Polymer-Derived Multishelled Mixed Ni-Co Oxide Microspheres for Robust and Selective Detection of Xylene. *ACS Appl. Mater. Interfaces* **2018**, *10*, 15314– 15321, DOI: 10.1021/acsami.8b03487

12 Kim, B.-Y.; Yoon, J.-W.; Kim, J. K.; Kang, Y. C.; Lee, J.-H. Dual Role of Multiroom-Structured Sn-Doped NiO Microspheres for Ultrasensitive and Highly Selective Detection of Xylene. *ACS Appl. Mater. Interfaces* **2018**, *10*, 16605– 16612, DOI: 10.1021/acsami.8b02412

13 Kim, B.-Y.; Ahn, J. H.; Yoon, J.-W.; Lee, C.-S.; Kang, Y. C.; Abdel-Hady, F.; Wazzan, A. A.; Lee, J.-H. Highly Selective Xylene Sensor Based on $NiO/NiMoO_4$ Nanocomposite Hierarchical Spheres for Indoor Air Monitoring. *ACS Appl. Mater. Interfaces* **2016**, *8*, 34603– 34611, DOI: 10.1021/acsami.6b13930

14 Yoon, J.-W.; Lee, J.-H. Toward Breath Analysis on a Chip for Disease Diagnosis Using Semiconductor-Based Chemiresistors: Recent Progress and Future Perspectives. *Lab Chip* **2017**, *17*, 3537– 3557, DOI: 10.1039/c7lc00810d

15 Kang, Y.; Kim, K.; Cho, B.; Kwak, Y.; Kim, J. Highly Sensitive Detection of Benzene, Toluene, and Xylene Based on CoPP-Functionalized TiO_2 Nanoparticles with Low-Power Consumption. *ACS Sens.* **2020**, *5*, 754– 763, DOI: 10.1021/acssensors.9b02310

16 Kou, D.; Ma, W.; Zhang, S.; Li, R.; Zhang, Y. BTEX Vapor Detection with a Flexible MOF and Functional Polymer by Means of a Composite Photonic Crystal. *ACS Appl. Mater. Interfaces* **2020**, *12*, 11955– 11964, DOI: 10.1021/acsami.9b22033

17 Nair, R. V.; Vijaya, R. Photonic Crystal Sensors: An Overview. *Prog. Quantum Electron.* **2010**, *34*, 89– 134, DOI: 10.1016/j.pquantelec.2010.01.001

18 Banerjee, M. B.; Pradhan, S.; Roy, R. B.; Tudu, B.; Das, D. K.; Bandyopadhyay, R.; Pramanik, P. Detection of Benzene and Volatile Aromatic Compounds by Molecularly Imprinted Polymer-Coated Quartz Crystal Microbalance Sensor. *IEEE Sens. J.* **2019**, *19*, 885– 892, DOI: 10.1109/JSEN.2018.2878926

19 Rianjanu, A.; Hasanah, S. A.; Nugroho, D. B.; Kusumaatmaja, A.; Roto, R.; Triyana, K. Polyvinyl Acetate Film-Based Quartz Crystal Microbalance for the Detection of Benzene, Toluene, and Xylene Vapors in Air. *Chemosensors* **2019**, *7*, 20, DOI: 10.3390/chemosensors7020020

20 Pejcic, B.; Myers, M.; Ranwala, N.; Boyd, L.; Baker, M.; Ross, A. Modifying the Response of a Polymer-Based Quartz Crystal Microbalance Hydrocarbon Sensor with Functionalized Carbon Nanotubes. *Talanta* **2011**, *85*, 1648– 1657, DOI: 10.1016/j.talanta.2011.06.062

21 Kimura, M.; Liu, Y.; Sakai, R.; Sato, S.; Hirai, T.; Fukawa, T.; Mihara, T. Detection of Volatile Organic Compounds by Analyses of Polymer-Coated Quartz Crystal Microbalance Sensor Arrays. *Sens. Mater.* **2011**, *23*, 359– 368

22 Nanto, H.; Dougami, N.; Mukai, T.; Habara, M.; Kusano, E.; Kinbara, A.; Ogawa, T.; Oyabu, T. A Smart Gas Sensor Using Polymer-Film-Coated Quartz Resonator Microbalance. *Sens. Actuators, B* **2000**, *66*, 16– 18, DOI: 10.1016/s0925-4005(99)00450-5

23 Peng, F. M.; Xie, P. H.; Shi, Y. G.; Wang, J. D.; Liu, W. Q.; Li, H. Y. Photoionization Detector for Portable Rapid GC. *Chromatographia* **2007**, *65*, 331– 336, DOI: 10.1365/s10337-006-0169-3

24 Çevik, E.; Dervisevic, M.; Gavba, A. R.; Yanik-Yildirim, K. C.; Abasiyanik, M. F.; Vardar-Schara, G. Amperometric Monooxygenase Biosensor for the Detection of Aromatic Hydrocarbons. *Sens. Lett.* **2016**, *14*, 234– 240, DOI: 10.1166/sl.2016.3646

25 Kadosaki, M.; Terasawa, T.; Tanino, K.; Tatuyama, C. Exploration of Highly Sensitive Oxide Semiconductor Materials to Indoor-Air Pollutants. *IEEJ Trans. Sensors Micromachines* **1999**, *119*, 383– 389, DOI: 10.1541/ieejsmas.119.383

26 Liaud, C.; Nguyen, N. T.; Nasreddine, R.; Le Calvé, S. Experimental Performances Study of a Transportable GC-PID and Two Thermo-Desorption Based Methods Coupled to FID and MS Detection to Assess BTEX Exposure at Sub-ppb Level in Air. *Talanta* **2014**, *127*, 33– 42, DOI: 10.1016/j.talanta.2014.04.001

27 Kadosaki, M.; Yamazaki, S.; Fujiki, S.; Tanino, K.; Tatsuyama, C. Development of SnO_2-Based Gas Sensors for Detection of Volatile Organic Compounds. *IEEJ Trans. Sensors Micromachines* **2001**, *121*, 395– 401, DOI: 10.1541/ieejsmas.121.395

28 Nasreddine, R.; Person, V.; Serra, C. A.; Le Calvé, S. Development of a Novel Portable Miniaturized GC for near Real-Time Low Level Detection of BTEX. *Sens. Actuators, B* **2016**, *224*, 159– 169, DOI: 10.1016/j.snb.2015.09.077

29 Lahlou, H.; Vilanova, X.; Correig, X. Gas Phase Micro-Preconcentrators for Benzene Monitoring: A Review. *Sens. Actuators, B* **2013**, *176*, 198– 210, DOI: 10.1016/j.snb.2012.10.004

30 Spinelle, L.; Gerboles, M.; Kok, G.; Persijn, S.; Sauerwald, T. Review of Portable and Low-Cost Sensors for the Ambient Air Monitoring of Benzene and Other Volatile Organic Compounds. *Sensors* **2017**, *17*, 1520, DOI: 10.3390/s17071520

31 Rigoni, F.; Tognolini, S.; Borghetti, P.; Drera, G.; Pagliara, S.; Goldoni, A.; Sangaletti, L. Enhancing the Sensitivity of Chemiresistor Gas Sensors Based on Pristine Carbon Nanotubes to Detect Low-ppb Ammonia Concentrations in the Environment. *Analyst* **2013**, *138*, 7392– 7399, DOI: 10.1039/c3an01209c

32 Li, J.; Lu, Y.; Ye, Q.; Cinke, M.; Han, J.; Meyyappan, M. Carbon Nanotube Sensors for Gas and Organic Vapor Detection. *Nano Lett.* **2003**, *3*, 929– 933, DOI: 10.1021/nl034220x

33 Yeow, J. T. W.; Wang, Y. A Review of Carbon Nanotubes-Based Gas Sensors. *J. Sens.* **2009**, *2009*, 493904, DOI: 10.1155/2009/493904

34 Mabrook, M.; Hawkins, P. Benzene Sensing Using Thin Films of Titanium Dioxide Operating at Room Temperature. *Sensors* **2002**, *2*, 374– 382, DOI: 10.3390/s20900374

35 Janudin, N.; Abdullah, N.; Yunus, W. M. Z. W.; Yasin, M. F.; Yaacob, M. H.; Saidi, N. M.; Kasim, N. A. M. Effect of Functionalized Carbon Nanotubes in the Detection of Benzene at Room Temperature. *J. Nanotechnol.* **2018**, *2018*, 2107898, DOI: 10.1155/2018/2107898

36 Das, R.; Pattanayak, A. J.; Swain, S. K. 7—Polymer Nanocomposites for Sensor Devices. In *Polymer Nanocomposites for Sensor Devices. Polymer-based Nanocomposites for Energy and Environmental Applications*; Jawaid, M., Khan, M. M., Eds.; Woodhead Publishing Series in Composites Science and Engineering; Woodhead Publishing, 2018, pp 205– 218.

37 Kerdcharoen, T.; Wongchoosuk, C. 11—Carbon Nanotube and Metal Oxide Hybrid Materials for Gas Sensing. In *Semiconductor Gas Sensors*; Jaaniso, R., Tan, O. K., Eds.; Woodhead Publishing Series in Electronic and Optical Materials; Woodhead Publishing, 2013; pp 386– 407.

38 Ndiaye, A.; Bonnet, P.; Pauly, A.; Dubois, M.; Brunet, J.; Varenne, C.; Guerin, K.; Lauron, B. Noncovalent Functionalization of Single-Wall Carbon Nanotubes for the Elaboration of Gas Sensor Dedicated to BTX Type Gases: The Case of Toluene. *J. Phys. Chem. C* **2013**, *117*, 20217– 20228, DOI: 10.1021/jp402787f

39 Zhang, W.; Sprafke, J. K.; Ma, M.; Tsui, E. Y.; Sydlik, S. A.; Rutledge, G. C.; Swager, T. M. Modular Functionalization of Carbon Nanotubes and Fullerenes. *J. Am. Chem. Soc.* **2009**, *131*, 8446– 8454, DOI: 10.1021/ja810049z

40 Edwards, E. R.; Antunes, E. F.; Botelho, E. C.; Baldan, M. R.; Corat, E. J. Evaluation of Residual Iron in Carbon Nanotubes Purified by Acid Treatments. *Appl. Surf. Sci.* **2011**, *258*, 641– 648, DOI: 10.1016/j.apsusc.2011.07.032

41 Ishihara, S.; Labuta, J.; Nakanishi, T.; Tanaka, T.; Kataura, H. Amperometric Detection of Sub-ppm Formaldehyde Using Single-Walled Carbon Nanotubes and Hydroxylamines: A Referenced Chemiresistive System. *ACS Sens.* **2017**, *2*, 1405– 1409, DOI: 10.1021/acssensors.7b00591

42 Yang, C.-M.; Kanoh, H.; Kaneko, K.; Yudasaka, M.; Iijima, S. Adsorption Behaviors of HiPco Single-Walled Carbon Nanotube Aggregates for Alcohol Vapors. *J. Phys. Chem. B* **2002**, *106*, 8994– 8999, DOI: 10.1021/jp025767n

43 Zhu, Z. An Overview of Carbon Nanotubes and Graphene for Biosensing Applications. *Nano-Micro Lett.* **2017**, *9*, 25, DOI: 10.1007/s40820-017-0128-6
44 Schroeder, V.; Savagatrup, S.; He, M.; Lin, S.; Swager, T. M. Carbon Nanotube Chemical Sensors. *Chem. Rev.* **2019**, *119*, 599– 663, DOI: 10.1021/acs.chemrev.8b00340
45 Gangoli, V. S.; Godwin, M. A.; Reddy, G.; Bradley, R. K.; Barron, A. R. The State of HiPco Single-Walled Carbon Nanotubes in 2019. *C* **2019**, *5*, 65, DOI: 10.3390/c5040065
46 Maultzsch, J.; Reich, S.; Thomsen, C. Raman Scattering in Carbon Nanotubes Revisited. *Phys. Rev. B: Condens. Matter Mater. Phys.* **2002**, *65*, 233402, DOI: 10.1103/physrevb.65.233402
47 Setaro, A.; Adeli, M.; Glaeske, M.; Przyrembel, D.; Bisswanger, T.; Gordeev, G.; Maschietto, F.; Faghani, A.; Paulus, B.; Weinelt, M.Preserving π-Conjugation in Covalently Functionalized Carbon Nanotubes for Optoelectronic Applications. *Nat. Commun.* **2017**, *8*, 14281, DOI: 10.1038/ncomms14281
48 Saito, R.; Hofmann, M.; Dresselhaus, G.; Jorio, A.; Dresselhaus, M. S. Raman Spectroscopy of Graphene and Carbon Nanotubes. *Adv. Phys.* **2011**, *60*, 413– 550, DOI: 10.1080/00018732.2011.582251
49 Smazna, D.; Rodrigues, J.; Shree, S.; Postica, V.; Neubüser, G.; Martins, A. F.; Ben Sedrine, N.; Jena, N. K.; Siebert, L.; Schütt, F.Buckminsterfullerene Hybridized Zinc Oxide Tetrapods: Defects and Charge Transfer Induced Optical and Electrical Response. *Nanoscale* **2018**, *10*, 10050– 10062, DOI: 10.1039/c8nr01504j
50 Krätschmer, W.; Lamb, L. D.; Fostiropoulos, K.; Huffman, D. R. Solid C60: A New Form of Carbon. *Nature* **1990**, *347*, 354– 358, DOI: 10.1038/347354a0
51 Garcia, S.; Rosenbauer, R. J.; Palandri, J.; Maroto-Valer, M. M. Sequestration of Non-Pure Carbon Dioxide Streams in Iron Oxyhydroxide-Containing Saline Repositories. *Int. J. Greenhouse Gas Control* **2012**, *7*, 89– 97, DOI: 10.1016/j.ijggc.2011.12.004
52 Liu, J.; Fu, S.; Yuan, B.; Li, Y.; Deng, Z. Toward a Universal "Adhesive Nanosheet" for the Assembly of Multiple Nanoparticles Based on a Protein-Induced Reduction/Decoration of Graphene Oxide. *J. Am. Chem. Soc.* **2010**, *132*, 7279– 7281, DOI: 10.1021/ja100938r
53 Zhou, X.; Zhang, J.; Wu, H.; Yang, H.; Zhang, J.; Guo, S. Reducing Graphene Oxide via Hydroxylamine: A Simple and Efficient Route to Graphene. *J. Phys. Chem. C* **2011**, *115*, 11957– 11961, DOI: 10.1021/jp202575j
54 Grosvenor, A. P.; Kobe, B. A.; Biesinger, M. C.; McIntyre, N. S. Investigation of Multiplet Splitting of Fe 2p XPS Spectra and Bonding in Iron Compounds. *Surf. Interface Anal.* **2004**, *36*, 1564– 1574, DOI: 10.1002/sia.1984
55 Bengtsson, G.; Fronæus, S.; Bengtsson-Kloo, L. The Kinetics and Mechanism of Oxidation of Hydroxylamine by Iron(III). *J. Chem. Soc., Dalton Trans.* **2002**, *12*, 2548– 2552, DOI: 10.1039/b201602h
56 Penza, M.; Rossi, R.; Alvisi, M.; Cassano, G.; Signore, M. A.; Serra, E.; Giorgi, R. Surface Modification of Carbon Nanotube Networked Films with Au Nanoclusters for Enhanced Gas Sensing Applications. *J. Sens.* **2008**, *2008*, 1– 8, DOI: 10.1155/2008/107057
57 Ellison, M. D.; Crotty, M. J.; Koh, D.; Spray, R. L.; Tate, K. E. Adsorption of NH_3 and NO_2 on Single-Walled Carbon Nanotubes. *J. Phys. Chem. B* **2004**, *108*, 7938– 7943, DOI: 10.1021/jp049356d
58 Mercuri, F.; Sgamellotti, A.; Valentini, L.; Armentano, I.; Kenny, J. M. Vacancy-Induced Chemisorption of NO_2 on Carbon Nanotubes: A Combined Theoretical and Experimental Study. *J. Phys. Chem. B* **2005**, *109*, 13175– 13179, DOI: 10.1021/jp0507290
59 Santucci, S.; Picozzi, S.; Di Gregorio, F.; Lozzi, L.; Cantalini, C.; Valentini, L.; Kenny, J. M.; Delley, B. NO_2 and CO Gas Adsorption on Carbon Nanotubes: Experiment and Theory. *J. Chem. Phys.* **2003**, *119*, 10904– 10910, DOI: 10.1063/1.1619948